Paper No.
4006

MODELING OF CORROSION OF STEEL IN CONCRETE WITH POTENTIAL-DEPENDENT CHLORIDE THRESHOLD

A. A. Sagüés, S.C. Kranc, and K. Lau
Dept. of Civil and Environmental Engineering, University of South Florida
4202 E. Fowler Ave. ENB118
Tampa, FL 33620

ABSTRACT

Deterministic forecast of corrosion damage progression in a reinforced concrete column was implemented in a one-dimensional model accounting for potential dependence of corrosion threshold, and macrocell coupling during the initiation and propagation stages. The damage projection was clearly sensitive to the choice of the activation zone size. The relative sensitivity became greater as the zone size decreased. Criteria for selection of this parameter need to be developed. The projected corrosion damage was significantly lowered when threshold dependence on potential was introduced, compared with a fixed threshold case. The damage projection was clearly sensitive to the choice of the activation zone size. The relative sensitivity became greater as the zone size decreased. Criteria for selection of this parameter are being developed.

Keywords: modeling, chloride threshold, potential, corrosion, steel, concrete

INTRODUCTION

Models to predict the evolution of corrosion damage in concrete reinforcing steel as a structure ages often use a single value for the critical chloride concentration for corrosion initiation (the chloride threshold, C_T), or a distribution of values fixed in time. However, there is increasing recognition[1-3] that the value of C_T depends on the value of the potential E of the passive steel with respect to the surrounding concrete. The dependence is such that C_T tends to increase as E becomes more cathodic(1). The first corrosion initiation event in a previously passive rebar assembly results in local shift of E toward more negative potentials. Galvanic coupling with the surrounding, still passive steel makes its potential more negative than before the onset of active corrosion. The value of C_T in that surrounding steel is therefore greater than it was for the spot first activated. Similar events occur as other portions of the assembly

(1) This dependence parallels the well-recognized relationship between pitting potential and chloride concentration in localized corrosion[4] but it may also reflect to some extent beneficial compositional changes (such as decrease in chloride content and pH elevation) at the steel-concrete interface[2].

become active. Thus, corrosion on many portions of the assembly is prevented until the chloride content reaches a local value of C_T that can be significantly greater than that encountered at the first spot that underwent activation. This phenomenon has received relatively little attention in current predictive models for corrosion damage in reinforced concrete, because of difficulty in quantitative implementation and, more notably, scarcity of data on the C_T -E relationship. Recently improved knowledge on the latter[1-2] put implementation of a potential-dependent threshold feature within reach of practical predictive models.

In previous work[5], two of the authors presented a detailed computational approach demonstrating incorporation of a potential dependent threshold in corrosion damage projections, plus integration of the initiation and propagation stages in one predictive model. That approach is revisited here taking into account new information in the C_T-E relationship and with emphasis on addressing modeling issues relevant to incorporation in practical forecasting models.

This earlier work was based on an available generic model of a partially submerged marine substructure column[6] having an assumed surface chloride concentration (C_S) profile. The system had rotational symmetry. A 2-dimensional finite difference computational grid divided the system into spatial nodes. Each steel node was associated with a corresponding steel area element. In that scheme the rebar assembly was assumed to be initially passive, undergoing anodic dissolution at a small current density i_p. If a portion of the assembly became active, anodic dissolution was assumed to proceed under active condition at a rate determined by assumed kinetic parameter values. The cathodic reaction, oxygen reduction, was assumed to proceed under combined activation-concentration polarization at rates also determined by assumed kinetic parameters, and an assumed oxygen diffusivity D_O profile. A *corrosion distribution module* computed the potential -E_C (referred to the steel assembly) and oxygen concentration C at every point in the concrete based on the passive/active character of the steel assembly at points of the steel/concrete interface. The value of E_C at each point of that interface was the local steel potential, E. A C_T-E functional relationship was also assumed. The calculated E profile as function of elevation for the initial moment (all-passive steel surface), had a nearly constant E value and a correspondingly nearly uniform C_T value. The evolution of chloride concentration as a function of time was calculated by means of a *chloride transport module* that assumed diffusional chloride transport. For the moment when C_T was reached at the first steel node to do so, the steel at that node was declared active. The corresponding redistribution of potentials and resulting corrosion rates was calculated using the corrosion distribution module. The C_T-E relationship was then applied to the newly developed E profile to determine the new distribution of C_T values. Every time an additional spot become active (due to the ever increasing chloride concentration at the rebar surface) the potential distribution became readjusted and so did the C_T distribution. As each spot entered the active corrosion condition, the corrosion distribution module calculated the local corrosion rate, which was integrated as a function of time and converted into local corrosion penetration by means of the *surface damage evaluation module*. This module also compared the local penetration with a value P_{crit} assumed to result in concrete cover cracking/spalling for the combination of steel bar (rebar) diameter and concrete cover used at that location of the system[7-8]. When P_{crit} was reached at a given steel node, the projected steel node area on the external concrete surface was counted as a damaged concrete area. The sum of damaged concrete area for the entire system as a function of time, divided by the total external concrete area, was defined as the *damage function* of the system.

The operation of the above approach was demonstrated by illustrations of evaluation of the effectiveness of corrosion mitigation procedures for the propagation stage of corrosion, including the use of submerged and surface galvanic anodes, and corrosion inhibitors. It is noted also that the approach powerfully integrates the initiation and the propagation stages of corrosion in a single predictive model. The model includes not only the effect of the regions already undergoing corrosion in delaying corrosion initiation elsewhere, but also the effect of macrocell development in accelerating/slowing corrosion propagation after activation of different zones of the steel assembly.

Inclusion of this modeling approach into forecasting schemes is expected to be an important step toward more realistic durability projections. However, some key issues need resolution before practical implementation. One of those issues is that the discretization used in the model establishes a minimum size of the steel surface that is activated in each initiation event. That size choice is expected to affect the resulting projected damage function to some degree. The corresponding sensitivity needs to be established and interpreted, together with evidence from the field, in choosing an appropriate activation zone size. Another issue of importance is the C_T-E relationship used in the calculations. Recent work[2] has shown that in the potential range of interest

$$C_T \sim C_{Ts} 10^{(E_P - E)/\beta_{CT}} \quad (1)$$

where E is the passive steel potential, C_{Ts} is the threshold value at a baseline potential E_P (i.e. in atmospherically exposed concrete, for passive steel that has not yet undergone any galvanic coupling to active steel), and β_{CT} is the characteristic inverse slope of the increase of C_T in an E-logC_T representation. There is a reasonable agreement on what representative values of E_P and C_{Ts} may be used in baseline calculations (e.g. E_P~-0.1 V CSE, C_{Ts}~0.004 × cement content). However, considerable uncertainty exists on the value of β_{CT}, which has been earlier estimated to be in the order of 0.1V [3] but for which recent work suggest as much as 0.5V. Due to the exponential dependence on β_{CT}, it is important to quantify sensitivity of the results to the choice of this parameter, to assess the impact on forecasting uncertainty and determine the need for additional experimental information. The work presented here concerns these two main issues.

MODELING

System

The system chosen for representation is a marine substructure, solid cylindrical reinforced concrete column partly submerged in seawater, of dimensions equivalent to those used when first introducing the potential-dependent threshold model[5]. For speed, an idealized one-dimensional model was used here to represent the column, comparable to that employed by the authors in related work[9]. As shown there, that approach captures most of the features of interest of the system with minimum computational burden. The column has a total height L, diameter Φ, and a single rebar mat placed at a cover depth X_C from the surface. The rebar mat, treated as a uniform sheet, has a total surface area of steel exposed to concrete equal to the external lateral column surface area multiplied by a Steel Factor S_F. The ends of the cylindrical column are considered to be isolated electrically and from the surrounding environment, and with no reinforcement. The column is assumed to be immersed in seawater to half its length. The concrete is approximated as an effectively homogeneous electrolytic

medium of resistivity ρ, effective chloride ion diffusivity D, and effective oxygen diffusivity D_O all of which are functions of elevation. Concrete on the lateral surface of the column is assumed to have developed very early a time-invariant chloride ion concentration C_S that is a function of elevation, and a time-invariant effective oxygen concentration C_{SO} treated as being constant with elevation.

The reinforcing steel is assumed to be the locus of an anodic metal loss reaction,

$$Fe \rightarrow Fe^{2+} + 2e^- \quad (2)$$

with a corresponding current density i_a, under two modalities: passive dissolution at a fixed small current density i_p, or active dissolution at a potential-dependent current density i_{aa} so that

$$i_a = i_p \quad \text{(passive case)} \quad (3a)$$

$$i_a = i_{aa} = i_{oa}\, 10^{(E-Eoa)/\beta a} \quad \text{(active case)} \quad (3b)$$

where i_{oa} is the nominal exchange current density, Eoa is the nominal equilibrium potential and β_a is the anodic Tafel slope. The steel is also assumed to support a single cathodic reaction, oxygen reduction:

$$O_2 + 2H_2O + 4e \rightarrow 4OH^- \quad (4)$$

which is considered for simplicity to occur under either a fully activation-controlled or a fully diffusion-limited conditions. Under full activation control the current density is

$$i_c = i_{ca} = i_{oc}\, 10^{(Eoc-E)/\beta c} \quad (5)$$

where i_{oc} is the nominal exchange current density, Eoc is the nominal equilibrium potential and β_c is the cathodic Tafel slope. Under full diffusional control the current density is

$$i_c = i_{cd} = 4\, F\, C_{SO}\, D_O / X_C \quad (6)$$

where 4 is the number of electrons to reduce O_2, F = 96.5 10^3 coul/equiv is Faraday's constant, C_{SO} is the oxygen concentration in the pore water at the external concrete surface, and D_O is the effective diffusion coefficient of O_2 in the concrete, scaled to match the concentration units used. The value of i_c is made to switch from i_{ca} to i_{cd} when the former exceeds the latter, creating a working approximation in lieu of the more computationally mixed polarization function[10].

For both anodic and cathodic reactions the corresponding reverse reactions are ignored as the potentials of interest are assumed to be far away from the respective equilibrium potentials.

Chloride transport module

The chloride concentration at the rebar depth C is calculated for regularly spaced times counting from the moment the structure is put in service. It is assumed for simplicity that

diffusion behavior is ideal, initial bulk contamination is zero, and that $Xc << \Phi$ (nearly flat wall condition) so at a moment t

$$C(t) = C_S \, (1\text{-}erf(Xc / (4Dt)^{1/2}) \quad (7)$$

Possible macroscopic effects of electric fields inside the concrete due to macrocell formation on chloride transport are ignored.

Corrosion distribution module

Calling x the distance along the column axis, defining and treating the problem as one-dimensional in a manner similar to that used in Ref.9 the charge conservation condition implies that

$$i_S = (\Phi/4 \, S_F) \, (\, \rho^{-1} \, d^2E/dx^2 + d(\rho^{-1})/dx \;\; dE/dx) \quad (8)$$

where $i_S = i_a - i_c$ is the net current density on the steel surface at elevation x , with ia being equal to i_{aa} or i_p depending on whether the local steel surface was declared active or passive respectively if the value of C was respectively above or below the value of C_T.

Solution of Eq. (8) to obtain i_S and E as function of x is conducted iteratively for each time t using finite differences on a 101-node equispaced array along the elevation direction. The declaration of whether a given node corresponds to active or passive steel is made using the value of C(t) from Eq. (7), and the local value of C_T calculated at each node per Eq.(1) using the value of E obtained at the end of the iterations conducted in the previous time step. The array of values of C_T remains unchanged during the iteration process. After iteration is complete the potential array is used as seed for the next time step potential calculations. It is noted that once steel at a given node is declared active, it remains so for all subsequent time steps. This is only a simplifying assumption that may be refined in future implementations of the modeling concept.

Surface damage evaluation module

The value of i_a for each node is integrated over time for each node, to obtain a cumulative anodic charge density (q_a) array. The anodic charge density at each node is Faradaically converted into a corrosion penetration depth P_C

$$P_C = A_{WFe} \, q_a \, / \, 2 \, F \, \rho_{Fe} \quad (9)$$

where A_{WFe} = 55.85 g/mol is the atomic weight of Fe and ρ_{Fe} = 7.8 g/cm^3 is the density of Fe.

For each time t and at each node the value of P_C is compared with the critical penetration depth P_{CRIT} that results in appearance of a crack/spall [(2)] at the surface of the

[(2)] The crack is assumed to be associated with simultaneous delamination of size comparable to the amount of external area corresponding to one rebar assembly node. The term "spall" is used here broadly to designate a delamination or the loss of concrete that would result if the delaminated portion were to fall off.

concrete[8] for the conditions encountered. If $P_C > P_{CRIT}$ the concrete at the position corresponding to the node is declared damaged. The damage is assumed to affect an elevation interval equal to the internodal distance. For the present simplified model, possible effects of the appearance of cracks in subsequent corrosion development in the column are not addressed. Importantly, the present model (as well as the earlier rotational-symmetry 2-dimensional approach) is limited to treat all points at a given elevation equally so lateral corrosion macrocells are not addressed either.

Summary of model inputs and outputs

Per the above, the model inputs consist of the column dimensions; rebar mat depth and steel factor; concrete resistivity, oxygen diffusivity and chloride diffusivity elevation profiles; steel electrochemical kinetic parameters; surface chloride and oxygen concentration profiles; and value of critical corrosion penetration. Basic model outputs as function of time are the chloride content at the rebar depth and the steel potential elevation profile. From those are derived the reaction current density profiles; corresponding declarations of active/passive steel condition profiles, and cumulative damage profile as well as integrated column damage. In the terminology of Tuutti's initial corrosion damage concepts [9], the corrosion initiation stage at each node ends with the declaration of active condition, and the propagation stage starts with the activation declaration and ends with the damage declaration when P_{CRIT} is exceeded.

Base case and variations.

The input parameter values are listed in Table 1. Figure 1 shows the corresponding parameter distribution as function of elevation. The dimensions chosen for the column, concrete cover and steel placement density are typical of those encountered in marine substructures. Chloride diffusivity was given for simplicity an elevation-independent representative value for these simulations but the choice is not limiting. In contrast, concrete resistivity and oxygen diffusivity were given values that were more realistic functions of elevation. For the waterline/high tide level the resistivity was assigned a low limit value. Above that level the resistivity was assumed to increase linearly with elevation; the limit values of those regimes were chosen to be roughly representative of actual observations in the field for low permeability concrete (with some adjustment for one-dimensional approximation, see note in Table 1) [11].

As noted in previous treatments of this system, as seawater has resistivity that is orders of magnitude smaller than that of concrete, the potential at external submerged portion of the column may be considered to be space-invariant [6]. For the one-dimensional model used here, all nodes for the submerged portion were assumed therefore for simplicity to share a common potential. That block of nodes, acting in unison, behaved as connected to the waterline node by a resistor of value determined by the resistivity assumed for the waterline level and the column dimensions and internodal spacing. Figure 1 shows for completeness the resistivity profile for the rest of the submerged zone, but that part of the profile does not enter in the calculations by virtue of the above simplifying assumption. Oxygen diffusivity was assumed to follow a similar pattern but inversely and on a logarithmic scale, to reflect the pronounced decreasing effect of water saturation on oxygen transport in concrete[12]. The range of values chosen is representative of those reported in the literature. As it is often encountered in marine applications, C_S was assumed to be greatest just above the waterline and decays with increasing elevation. C_S was assumed to follow a simple decreasing linear variation with increasing elevation above high tide, and the end values given in the Table are representative

of regimes encountered in Florida bridges. A nominal value of C_S equal to 3/5 of the waterline/high tide elevation Cs value was assumed for the submerged region, where no evaporative chloride accumulation occurs on the concrete surface. The chosen value of C_{TS} is a commonly assumed conservative value for steel in atmospherically exposed concrete, where the passive steel potential is similar to the choice of E_P used. While the above material properties and boundary conditions are loosely representative of some field conditions, it is emphasized that the values were chosen mainly for illustration of the modeling concept and not to match the behavior of a specific actual system.

Polarization kinetic parameters values for the corrosion reactions are generally plausible amounts similar to those used in previous modeling approaches[6]. For the baseline case a threshold potential dependence β_{CT} value of 0.4V/decade was assumed, reflecting a regime suggested by a recent literature compilation[2]. Variations were slopes of 0.2 V/decade and 0.1 V/decade reflecting increasingly optimistic but also more uncertain scenarios. The size of the activation zone in the baseline case was that corresponding to one internodal space, which for the column dimensions used corresponded to 0.38 m^2. Variations included active zones equal to ½, 2 and 3 times the surface area of the baseline case. The larger cases were simulated by declaring one or two adjacent nodes respectively to be active upon activation of an individual node. The ½ case was simulated by conducting calculations with twice the number of longitudinal nodes, but keeping the conductance between the waterline node and the submerged portion equal to that used for the other configurations. The kinetic parameters representing potentials were chosen to correspond to the copper-copper sulfate (CSE) reference electrode scale. See note in Table 1 for sign conventions.

The calculations cover the period from 0 to 60 years of age, using a 0.25 years time step. That time step value was found to be fine enough to avoid in most cases multiple activation declarations of adjacent zones in a single time step. In the few instance where two or more adjacent zones were found to have exceeded the value of C_T during a single time step, only the zone with the greatest excess was allowed to become active. The procedure was extended with appropriate allowance to the active zone variation cases. It is noted however that the submerged portion nodes were always treated for simplicity as a single unit and subject to simultaneous activation.

RESULTS AND DISCUSSION

The surface chloride concentration profile chosen for these illustrations causes chloride accumulation at the rebar surface to be fastest at the waterline elevation. Consequently, steel activation happens there first. Figure 3 shows the steel potential-elevation profiles for the base case at ages 24y, 27 y, 54y and 60y. The 24 y graph shows also (dashed line) the initial potential profile when the entire assembly was passive. Consequently, and for the polarization parameters chosen, the assembly was initially at a nearly constant potential of ~-0.155 V which is typical of passive steel in concrete. That condition was maintained until the end of year 24, when the waterline node was the first to become active. At that time the steel at that node became a net anode and the potential profile changed into that indicated by the solid line in the 24 y graph. The steel there developed a distinctly negative potential, as commonly observed upon local activation. The potential depression was projected also on the nearby, still passive nodes, reflecting macrocell galvanic coupling. The effect died off above water with distance from the active node also consistent with macrocell coupling in a resistive electrolyte. On the side of the submerged nodes the potential drops immediately due to their much larger combined surface area and assumed equipotential condition. The steel at the active spot

underwent corrosion at a high rate as a consequence of this coupling. During the next 3 years chloride concentration built up to higher levels in the surrounding passive nodes, even exceeding the initial C_T value, but activation did not take place in those nodes because the C_T values had increased due to the local potential depression. Instead, the next activation event (year 27) took place at a higher elevation where the preventing effect from the polarization induced by the first anodic zone was lower. That event occurred later because at that higher elevation the surface concentration was lower. That second activation created a second negative peak in the potential profile, with associated potential depression and C_T increase in the nearby passive steel nodes.

The next events of note included additional activations above the waterline as the ever increasing chloride concentration exceeded the local C_T value, but always some distance away from nodes already active as those delayed corrosion initiation around them. That condition is illustrated in the figure for year 54. Just after year 54 the entire submerged zone became active reflecting the lower, but still significant value of C_S present there. The steel activation there resulted in potentials that were the most negative in the system, because the cathodic rate there can only be very small due to the low oxygen diffusivity, causing the reaction to be fully concentration limited. Consequently the corrosion rates below the waterline were very low. That condition is shown in the figure for year 60 (end of the simulation), where the column potential profile had reached a mature pattern with multiple corroding zones above the waterline, separated by intermediate positions were the cathodic prevention effect delayed activation over a long time frame. The potentials calculated for the active and passive portions generally approximate those encountered in actual corroding marine structures. However, for the exploratory purposes of this paper no attempt was made to refine the selection of kinetic parameters to develop a direct comparison to any specific system.

Figure 3 (left) details for the base case and for every elevation the moment at which the corresponding node became active (open circle), corresponding to the end of the initiation and beginning of the propagation periods there. The solid circle corresponds to the moment at which damage is declared for that node, or end of the propagation period. For clarity, a grey line joins both points at each relevant elevation. The first node to be activated (at the waterline) became so at 24.y and damage declaration (P_{CRIT}=0.01 cm) was reached at 27 y. Thus, the time-averaged corrosion rate for that node for the intervening period was 33 μm/y. This rate is over an order of magnitude higher than the value corresponding to the limiting current density for oxygen reduction there, so the anodic reaction at this node was driven mainly by macrocell coupling with the surrounding passive nodes both above and below water. The distance between the two symbols for the other active nodes provides likewise an inverse indicator of the local corrosion rate. It is noted that for the submerged zone no damage declaration occurred up to the 60 y end of the realization. This behavior agrees with the very low oxygen diffusion-limited corrosion rate prevalent at those locations, for which macrocell coupling with the rest of the system is weak. However, it is noted also that for these simplified simulations the entire submerged region is treated as evolving simultaneously. However, localized corrosion behavior could easily occur there too and simulation of such and its consequences is being investigated in continuation work[3].

[3] The extent of corrosion penetration needed to create cracks/spalls in the wetter concrete in the submerged zone could be greater than above water. Moreover, the mode of damage present below water may be different as well. Modeling of that behavior is made more uncertain by the relatively small amount of information on underwater corrosion of steel in concrete[8].

Figure 4 (top) shows the cumulative damage function for the Base case ("Single"). Each damage event involves a single node, or ~1% of the total column surface. At 60y, the damage percentage was ~11%. It is noted that since that damage affects until then only the above-water half of the column, the relative damage there is actually ~22%. The damage function has an uneven, stepwise quality corresponding to the time difference between successive activation and propagation events, and the relative corrosion-preventing throwing power at different elevations according to the local corrosion rate and concrete resistivity. It is emphasized that the projection is entirely deterministic and not the result of a probabilistic assignment of corrosion initiation events or propagation rates, as it is used in other forecasting approaches[13,14]. It is also noted that the simplified one-dimensional model generally approximated the results of the 2-dimensional rotational symmetry model used in our previous work [5]. Model parameters and system configuration were chosen here to be comparable to those used in the earlier work to facilitate such comparison of results as an additional check.

Figure 4 (top) shows also the result of variations where each activation event affects only ~0.5% of the surface ("Half"), ~2% ("Double") and ~3% ("Triple"). In answer to one of the questions addressed in this paper, the damage projection was clearly sensitive to the choice of the activation zone size as the zone size decreased. As this parameter cannot at present be bounded *a-priori*, in principle the assumed sizes could be arbitrarily small values. If the observed trend were to continue, accordingly smaller projected damage would result. It is speculated that a lower zone size limit may be reached, where the decrease in amount of damage associated with smaller individual corroded zones is compensated by an increase in number of nearby activation events (because the smaller zones will polarize less the surrounding passive steel). The validity of that hypothesis needs to be examined by analyses with finer discretizations and multidimensional models (addressing macrocell behavior for regions at the same elevation) some of which have been initially implemented[15]. Alternative selection of activation zone size based on experimental observations needs to be considered as well. Investigation to those ends is in progress.

Figures 3(right) and 4(bottom) shows results relevant to the other issue investigated here, namely the effect of the threshold potential dependence slope β_{CT} on the damage projection. Figure 3(right) shows that with no threshold dependence (fixed C_T = 0.71 kg/m^3) activation still occurs first at the waterline node, and at nearly the same time as in the base case (the small difference is due to the open circuit potential of the all-passive assembly being some 30 mV lower than the assumed E_P value). Unlike in the Base case, activation of the nearby nodes at increasingly higher elevations occurs very soon as no protection is derived from the first or subsequent active zones. Thus a continuum of active steel tends to form with less macrocell action compared with the base case. Consequently the local corrosion rates tend to be limited by oxygen supply, which is less at the lower elevations according to the assumed oxygen diffusivity profile. Thus, the time interval between activation and damage declaration at the lower above water locations is much greater than in the base case, to the extent that for many of those nodes damage was not reached by year 60. An exception is the waterline node, which experienced efficient galvanic coupling with the still passive region below waterline and consequently reached the damage condition only about 3 years after activation. At increasingly higher elevation oxygen supply was much less limited and the damage condition was reached increasingly sooner after activation. Although the first subsequent damage declarations were reached later than in the base case, there were many more active nodes than in the base case. Thus for the fixed threshold case the damage

function rises comparatively much faster even though it starts accelerating somewhat later than in the cases with potential dependent threshold.

The outcome was, as expected, sensitive to the choice of β_{CT}, with slower damage progression the smaller the slope was. Notably in view of the exponential dependence of C_T on β_{CT}, for the conditions examined the variation of projected damage after 60y service differed by only roughly a factor of two when varying β_{CT} from 0.4 V to 0.1 V, a range considered in the Introduction to reflect available data and proposed working amounts. That sensitivity may be viewed as being only moderate compared with the other uncertainties involved at present in typical damage projections for reinforced concrete. Further cases are being analyzed at present to explore this issue over a broader range of key concrete, polarization and environmental parameters.

The present paper describes exploratory applications of a novel approach for forecasting damage due to corrosion of steel in concrete. It is noted that the calculations here were performed for agility using only a simplified one dimensional model, which does not allow for interaction between active and passive zones at different perimeter positions at a given elevation. However, important insight on key durability factors was readily obtained. Continuation work will take advantage of output from more detailed models[15] toward developing implementation of threshold potential dependence and integrated initiation-propagation modules in practical forecasting procedures.

CONCLUSIONS

Deterministic forecast of corrosion damage progression in a reinforced concrete column was implemented in a one-dimensional model accounting for potential dependence of chloride corrosion threshold concentration, and macrocell coupling during the initiation and propagation stages. The results successfully approximated those of our earlier work employing a 2-dimensional rotational symmetry model.

The projected corrosion damage was significantly lowered when threshold dependence on potential was introduced, compared with a fixed threshold case. The damage projection depended on the choice of the slope of the relationship between log of threshold concentration and potential. However, within the plausible range of slope values, the sensitivity to the choice of slope was moderate compared with the effect of other model uncertainty sources.

The damage projection was clearly sensitive to the choice of the activation zone size. The relative sensitivity became greater as the zone size decreased. Criteria for selection of this parameter need to be developed.

ACKNOWLEDGEMENT

This investigation was partially supported by the Florida Department of Transportation. The opinions and findings stated here are those of the authors and not necessarily those of the funding agency.

REFERENCES

1 C. Alonso, M. Castellote, C. Andrade, Electrochim. Acta Vol. 47, p. 3469, 2002.

2 F.J. Presuel-Moreno, A.A. Sagüés and S.C. Kranc, Corrosion Vol 61, p428, 2005.

3. L. Bertolini, F. Bolzoni, T. Pastore and P. Pedeferri, "New Experiences on Cathodic Prevention of Reinforced Concrete Structures", pp. 390-398 in Corrosion of Reinforcement in Concrete Construction", C. Page, P. Bamforth and J. Figg, Eds., Society for Chemical Industry, Special Publication No. 183, London, 1996.

4. Z. Szklarska-Smialowska, Pitting Corrosion of Metals. NACE, Houston. 1986.

5. "A.A. Sagüés and S.C. Kranc, Model for a Quantitative Corrosion Damage Function for Reinforced Concrete Marine Substructure" , in Rehabilitation of Corrosion Damaged Infrastructure, p.268, Proc., Symp. 3, 3rd. NACE Latin-American Region Corrosion Congress, P.Castro, O.Troconis and C. Andrade, Eds., ISBN 970-92095-0-7, NACE International, Houston, 1998.

6. S.C. Kranc and A.A. Sagüés, Corrosion, Vol. 50, p.50, 1994.

7. C. Andrade, C. Alonso, J. Rodriguez and M. Garcia, "Cover Cracking and Amount of Rebar Corrosion: Importance of the Current Applied Accelerated Tests", pp. 263-273 in Concrete Repair, Rehabilitation and Protection, R. Dihr and M. Jones, Eds, E&FN Spon, London, 1996.

8. A. Torres-Acosta and A. Sagüés, ACI Materials Journal, Vol. 101, p.501, 2004.

9. F. J. Presuel-Moreno, S.C. Kranc, A.A. Sagüés, Corrosion, Vol. 61, p.548, 2005

10. H. Kaesche, Metallic Corrosion. NACE, Houston. 1996.

11. A.A. Sagüés et al, "Corrosion Forecasting for 75-Year Durability Design of Reinforced Concrete," Final Report to Florida D.O.T. WPI 0510805. Dec. 2001, Available online, www.dot.state.fl.us.

12. K. Tuutti, "Corrosion of Steel in Concrete" (ISSN 0346-6906), Swedish Cement and Concrete Research Institute, Stockholm, 1982.

13. A.A. Sagüés, Corrosion, Vol. 59, p.854, 2003.

14. E. Bentz, ACI Materials Journal, Vol. 100, p.391, 2003.

15. S.C. Kranc and A.A. Sagüés, "Development of Damage Functions to Predict the Durability of Steel Reinforced Concrete Structural Elements", presentation at Corrosion-Conference on Understanding Corrosion Mechanisms in Concrete, M.I.T., Cambridge, Mass., 27-31 July, 1997.

TABLE 1
MODEL PARAMETERS*

(Refer to Figure 1 for key)

Steel Cover	Xc =	10.5 cm
Column diameter	Φ=	105 cm
Column Length	L=	1200 cm
Concrete Resistivity	ρ_H=	$2\ 10^5$ ohm-cm
	ρ_L=	$4\ 10^4$ ohm-cm
Oxygen Diffusivity	D_{OH}=	10^{-3} cm^2/sec
	D_{OL}=	10^{-5} cm^2/sec
Chloride Diffusivity	D=	$2\ 10^{-8}$ cm^2/sec
O_2 Surface Concentration	C_{SO}=	$2.5\ 10^{-7}$ mol/cm^3 (in pore water)
Cl^- Surface Concentration	C_{SH}=	15 Kg/m^3
	C_{SW}=	9 Kg/m^3
	C_{SL}=	0 Kg/m^3
Chloride Threshold Parameters	C_{TS}=	0.71 Kg/m^3
	E_p=	-128 mV
	β_{CT} =	400 mV (Base); 200 mV, 100 mV, Fixed C_T (Variations)

Polarization Parameters**	E_0 (-mV CSE)	i_0 (A/cm^2)	Tafel Slope (mV)
Iron Dissolution	-780	$1.875\ 10^{-8}$	60
Oxygen Reduction	+160	$6.25\ 10^{-10}$	160

Steel Passive Current Density	$i_p = 0.058\ 10^{-6}$ A/cm^2
Critical Corrosion Penetration	P_{CRIT} = 0.01 cm
Active Zone Size	1 node (Base); ½ node, 2 nodes, 3 nodes (Variations)

* To provide a rough check on model operation, system parameters and configuration were chosen to be comparable to those used in earlier 2-dimensional cylindrical geometry calculations presented in Ref. 5. Concrete resistivity was assigned twice the earlier value to compensate somewhat for differences in the effective conductive path resulting from the assumptions used here.

**Potentials are presented in this table and the results using the usual electrochemical convention where the rate of anodic reactions increases as the potential becomes more positive. Equations in the text however address potentials in the electrolyte with effectively the opposite convention.

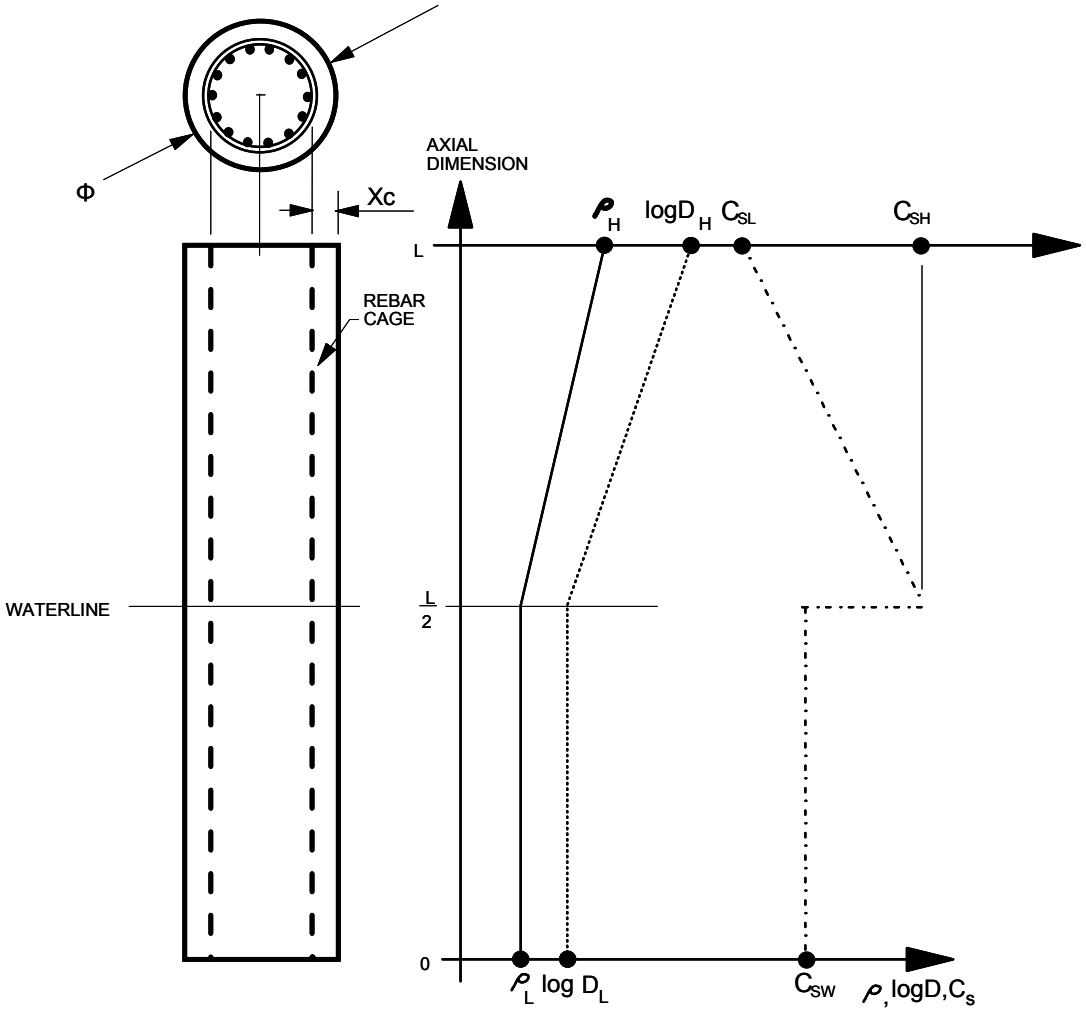

FIGURE 1 - System modeled

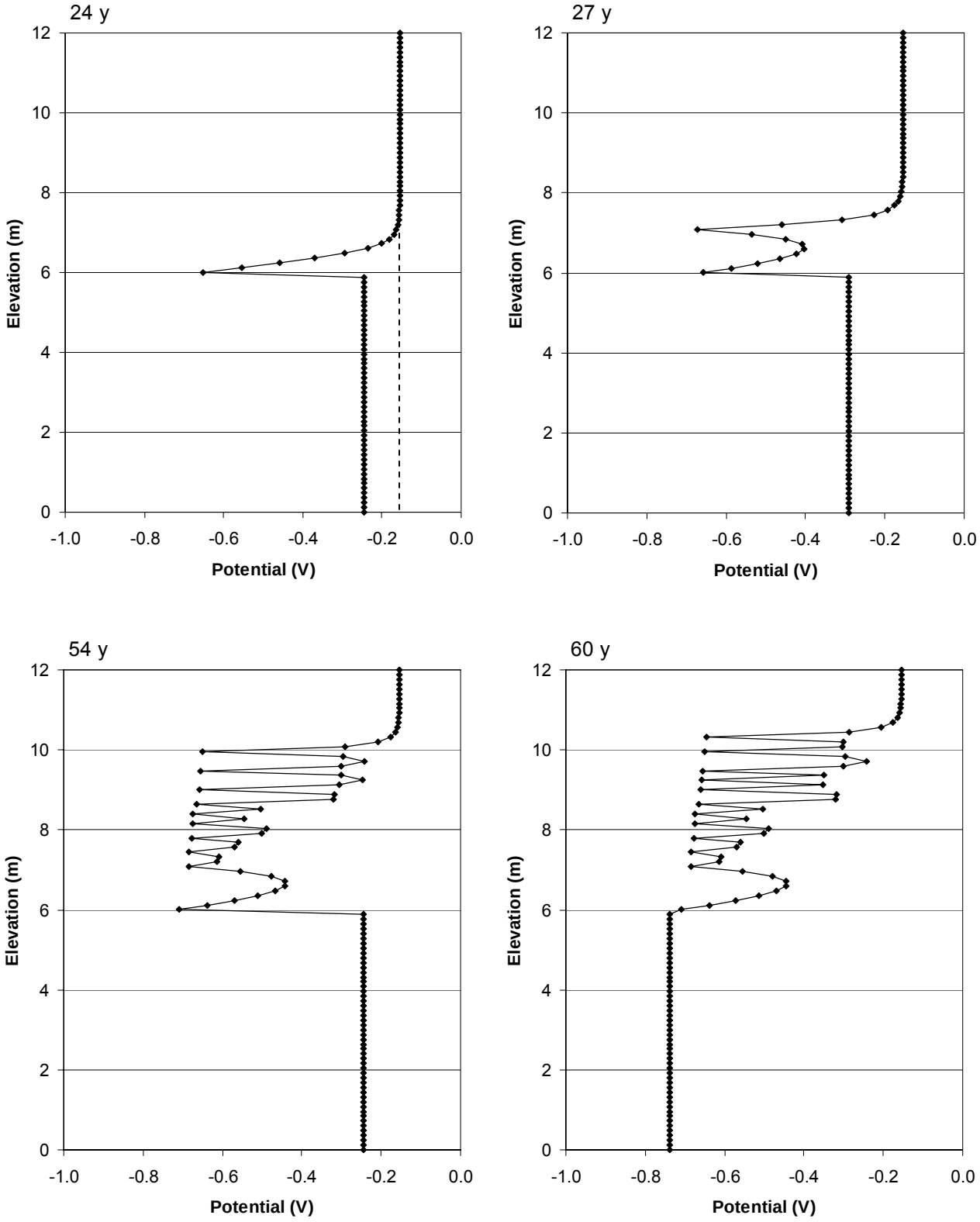

FIGURE 2 - Evolution of potential-elevation profile as function of age, Base case. The dashed line is the initial potential profile of the all-passive assembly. 24 y: first activation event. 27y: second event. 54 y: just before activation of submerged portion. 60y: mature pattern.

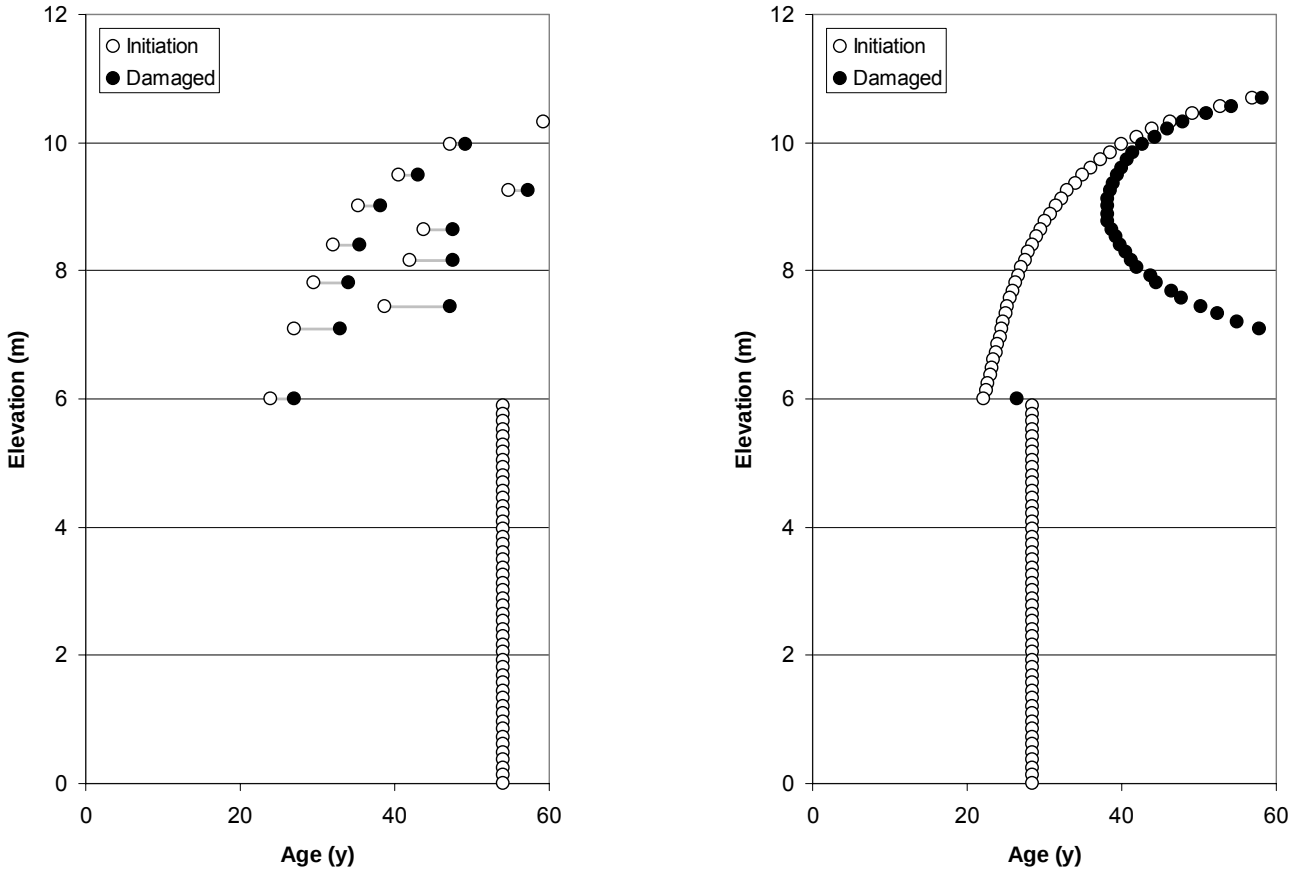

FIGURE 3 - Left: Base case initiation and damage declaration events. Lines joining both events shown for clarity. Right: Fixed threshold case

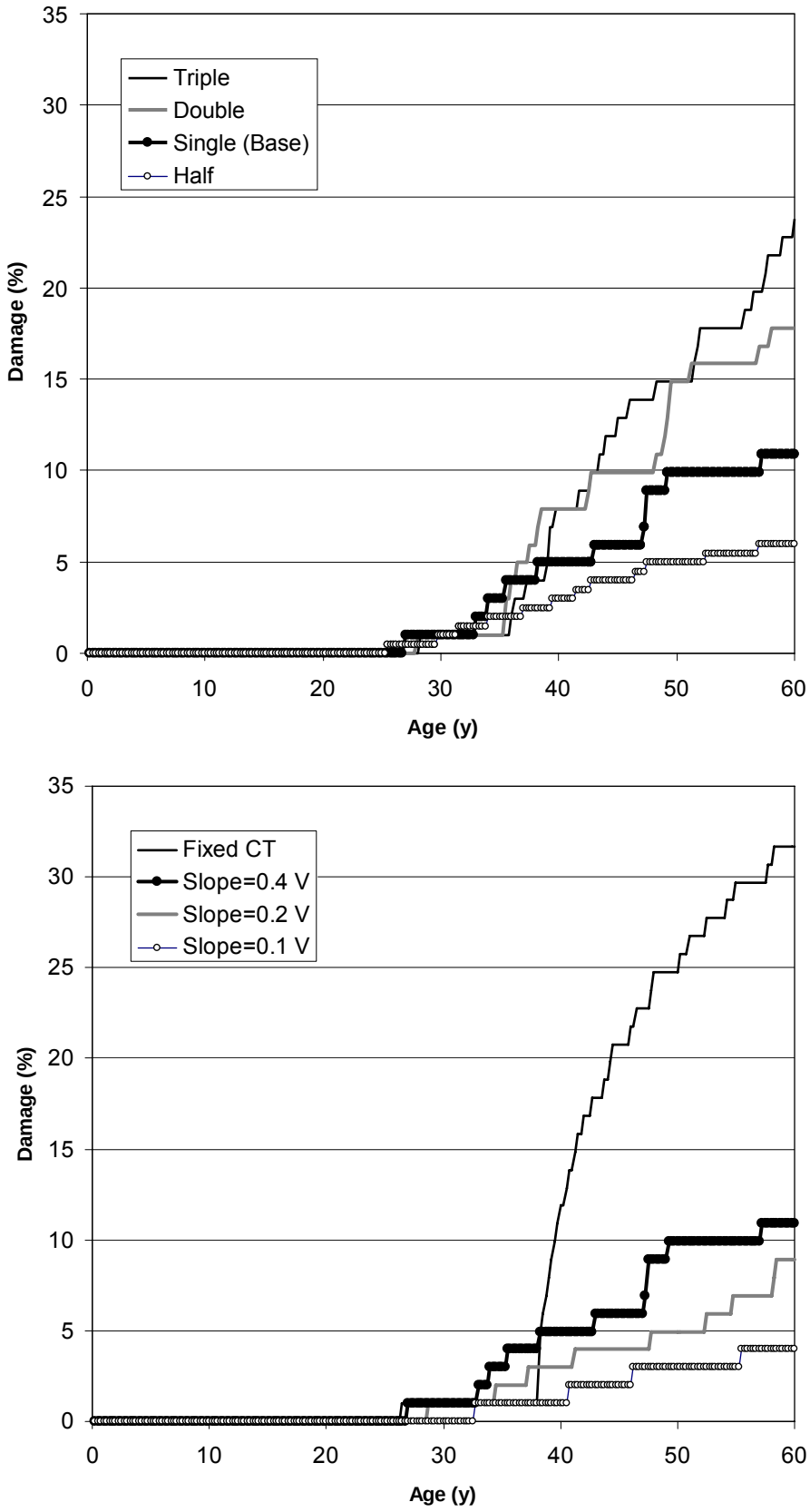

Figure 4 - Top: Damage projections for Base case (Bold, "Single") and active zone size variations. Bottom: Damage projections for Base case (Bold, "Slope=0.4V") and slope variations including Fixed C_T.